CERN-ACC-NOTE-2018-0036
xavier.buffat@cern.ch

Status of the studies on collective effects involving beam-beam interactions at the HL-LHC

X. Buffat, L. Barraud, E. Métral, A. Ribes Metidieri,
CERN, Geneva, Switzerland,
J. Barranco, P. Gonçalves, T. Pieloni, C. Tambasco,
EPFL, Lausanne, Switzerland

Abstract

This note summarises the status of the studies on the coherent beam-beam effects in the HL-LHC project. It is shown that the obit, tune, chromaticity and dynamic β effects due to head-on and long-range beam-beam interactions are tolerable without dedicated mitigations in the nominal scenario. The stability of coherent beam-beam modes under the influence of the beam coupling impedance is evaluated, as well as the impact of the beam-beam induced tune spread on the Landau damping of single beam head-tail modes of oscillation. Since the beam stability is marginal at the end of the squeeze for the ultimate scenario, it is suggested to use the ATS optics to increase the effect of the octupoles at constant current, thus providing sufficient margins. Measurements suggesting that the transverse damper noise has to be significantly reduced to allow for operation with large beam-beam parameter are shown.

Geneva, Switzerland
May 25, 2018

Contents

1 Introduction

The High-Luminosity upgrade of the Large Hadron Collider (HL-LHC) [Apollinari:2284929] relies on different aspects in order to achieve the desired increase of the luminosity which have a significant impact on the coherent beam-beam forces, affecting in particular the bunch by bunch orbits, the optics and the beam stability. The current knowledge of these effects as well as the plans to address the remaining unknowns are detailed in this note. Unless stated otherwise, all studies are based on the nominal parameters detailed in [1].

2 Pacman effects

2.1 Orbit

Based on the dipole field generated by a long-range beam-beam interaction [2] and the corresponding orbit distortion [3], we find that for N_{LR} interactions at a location $s = 0$ where the optics functions do not vary significantly the orbit distortion is given by:

$$\Delta x(s) = \frac{N_{LR} N r_p}{d \ \sin(\pi Q)} \sqrt{\frac{\beta(s)}{\gamma \varepsilon}} \sin(\phi(s) - \pi Q), \tag{2.1}$$

$$\text{or } \frac{\Delta x(s)}{\sigma(s)} = \frac{N_{LR} N r_p}{d \ \varepsilon \ \sin(\pi Q)} \sin(\phi(s) - \pi Q), \tag{2.2}$$

where we have introduced the optical $\beta(s)$ function with the corresponding phase advance $\phi(s)$, the relativistic γ factor, the bunch intensity N, the normalised transverse emittance ε, the machine bare tune Q, the classical proton radius r_p and the normalised separation between the beams at the location of the long-range beam-beam interaction d. The optics function refer to the beam under consideration, the optics function of the opposing beam do not impact the strength of the long-range interactions in the approximation $d >> \sigma$. The normalised separation is almost constant in the common chamber before the separation dipole D1, and can be approximated by [4]:

$$|d| = \sqrt{\frac{\beta^* \gamma}{\varepsilon}} \theta, \tag{2.3}$$

with θ the full crossing angle between the beams and β^* the optical function at the IP. After the D1, the separation increases rapidly and will therefore be neglected in this analytical estimation. Nevertheless, all interactions in the common chamber until the D2 are considered in the self-consistent simulations. Due to the large β function, the phase advance is almost constant in the common chamber except at the IP where the phase advance varies by π between the two sides of the IP due to the strong focalisation at the IP. The resulting orbit effects in a single interaction region are illustrated in Fig. 1. The peak-to-peak spread in

orbit is maximum at the IP, nevertheless the two beams behave symmetrically around the IP, therefore the orbit effect does not result in a luminosity loss, but rather a displacement of the luminous centroid. The symmetry between the two beams is not fully achieved in realistic configurations, nevertheless TRAIN simulations confirm that the residual separation remains negligible. On the other hand, the orbit spread generated outside of the IP can be detrimental e.g. for the luminosity of other IPs. The maximum normalised orbit spread outside of the interaction region is given by:

$$\max_s \left(\frac{\Delta x(s)}{\sigma(s)} \right) = \frac{N_{LR} N r_p}{d \ \varepsilon \ \sin(\pi Q)}. \tag{2.4}$$

This orbit spread is illustrated in the nominal HL-LHC configuration at the start of collision in Fig. 2, where the effect of beam-beam interactions in all IPs is taken into account. The closed orbit of all bunches is evaluated taking into account the non-linear coherent force between each bunch pair, using an iterative algorithm converging to a fully self-consistent solution. The orbit distortion of each individual bunch is expressed in normalised radial coordinates in phase space at IP1, providing an estimate of the amplitude of effect expected elsewhere in the ring:

$$r^2 = \Delta X^2 + \Delta X'^2, \text{ with } \Delta X = \frac{\Delta x}{\sigma_x} \text{ and } \Delta X' = \frac{\Delta x'}{\sigma_{x'}}. \tag{2.5}$$

The behaviour of the orbit spread in the horizontal plane is mainly driven by the long-range interactions in IPs 1 and 8 and respectively 2 and 5 in the vertical plane due to the crossing angle plane. While most bunches experience the beam-beam interactions in all IPs, two sets of bunches stand out since they do not collide in either IPs 2 or 8 (slots from 800 to 990 and from 2590 to 2770). On top of that, the gaps in between the trains leads to a variety of Pacman bunches missing one to all long-range interactions on one side of the different interaction regions. In order to compare the amplitude of this effect in different machine and beam configurations, we report in Tabs. 1 and 2 the maximum peak-to-peak difference between the bunch positions along the ring taking into account the beam-beam interactions in the two main IPs, $\max \Delta X_{1,5}$, as well as taking into account all interactions, $\max \Delta X_{tot}$. While the first is driven by long-range interactions in the two main IPs, the second contains also the effect of the long-range and the offset interactions at IPs 2 and 8. The maximum orbit spread is systematically lower than the absolute sum of the contributions of the different IPs, due to the different phase advance between the IPs. The contributions of the individual IPs to the orbit spread obtained with TRAIN are within $\pm 20\%$ of the prediction using Eq. 2.4, which is expected since the formula does not take into account the variation of the orbit and of the β function in the triplets and neglects the self-consistency.
In terms of aperture, the orbit spread obtained exceeds the 2 mm tolerance for static offsets in the triplets [5]. Detailed studies are therefore required in order to fully evaluate the impact of such effects on the different failure scenarios.
The impact on the luminosity at the different IPs is marginal, since it depends on the r.m.s. orbit spread at the IP rather than the peak-to-peak difference shown in Tabs. 1 and 2. The relation between the peak-to-peak and the r.m.s. is mainly driven by the number of Pacman bunches, nevertheless for all filling schemes the r.m.s. contribution is 20% to 25% of the peak-to-peak value, representing a marginal reduction of the luminosity.
The induced voltage in the crab cavity, as well as the corresponding power load were found to be acceptable [6].

2.2 Tune

The tune shift due to head-on interactions for round beams without crossing angle is given by [2]:

$$\Delta Q_{HO} = -\frac{N r_p}{4\pi\varepsilon}, \tag{2.6}$$

in both planes. With nominal HL-LHC parameters, taking into account a reduction of 6% due to the remaining effective crossing angle, we obtain a total tune shift of $\Delta Q_{HO} = -0.02$ for IPs 1 and 5. The interaction in IPs 2 and 8 are offset for levelling purposes and the corresponding tune shift is reduced w.r.t. the one of the main IPs [1, 9].
The tune shift due to long-range interactions on one side of an IP can be approximated by [2]:

$$\Delta Q_{LR} = \pm N_{LR} \frac{N r_p}{2\pi\varepsilon d^2} \tag{2.7}$$

which ranges from $\approx 7 \cdot 10^{-4}$ for the nominal scenario at the start of collision to $\approx 1.2 \cdot 10^{-3}$ for the ultimate scenario. The tune shift is positive in the plane of the crossing angle, and negative in the other. Thanks to the alternating crossing angles in the two main IPs, their contributions to the total tune shift is

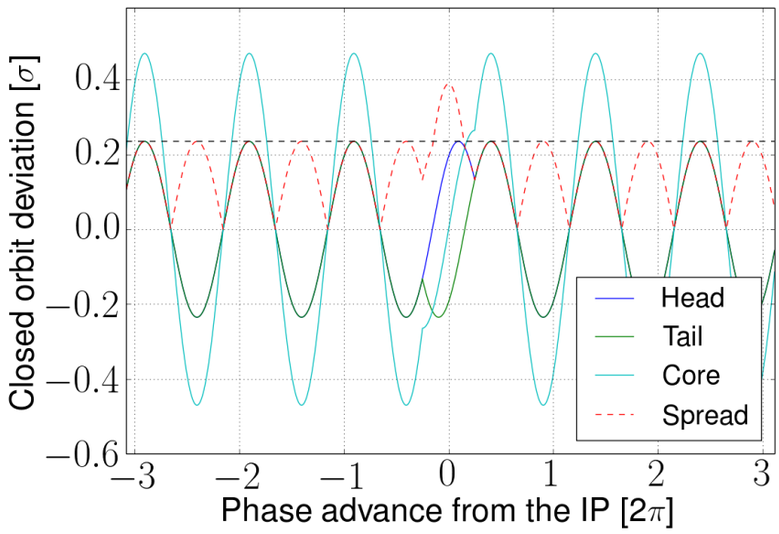

Figure 1: Normalised orbit change due to 18 long-range beam-beam interactions at $\pi/2$ on each side of the IP, for an intensity of $2.2 \cdot 10^{11}$ protons per bunch and a transverse emittance of 2.5 μm. The bunches at the head and tail experience the long-range interaction only on one side of the IP, whereas the ones in the core of the train experience all of them, resulting in a non-correctable peak-to-peak orbit spread shown in dashed red. The dashed black line corresponds to Eq. 2.4.

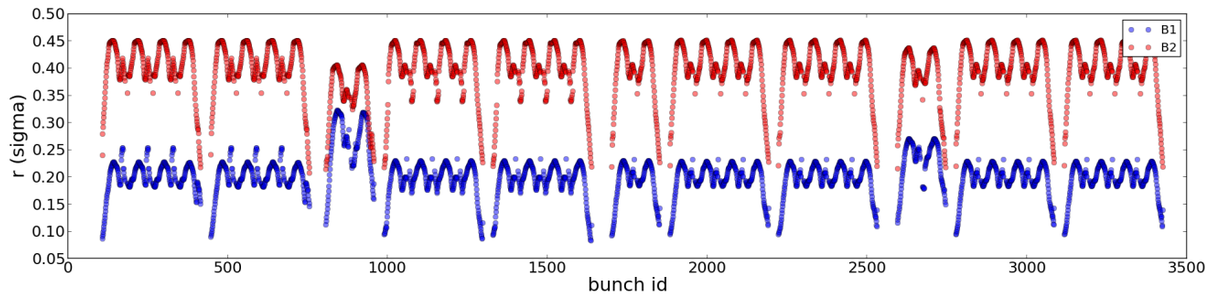

(a) Horizontal

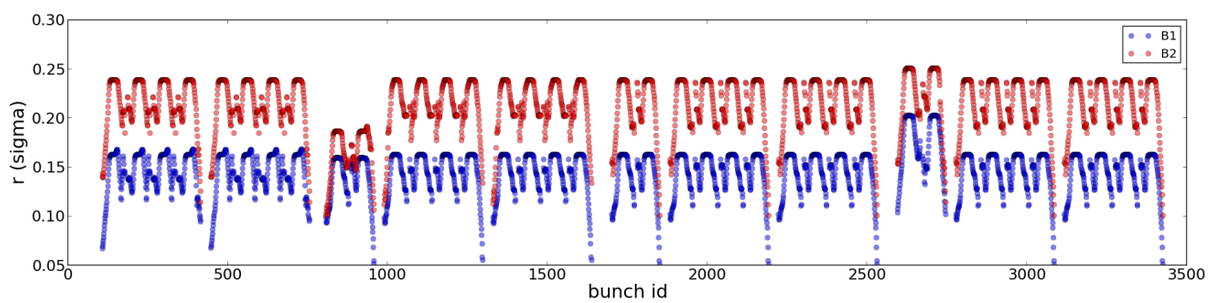

(b) Vertical

Figure 2: Bunch-by bunch orbit at the start of collision for the nominal configuration with the standard filling scheme [7, 8]. The radius computed in the normalised phase space at IP1 is expressed in beam size. While the unperturbed orbit is at 0, it is expected that the orbit will be re-optimised once in collision such that the average separation at the IPs is minimised, thus maximising the luminosity.

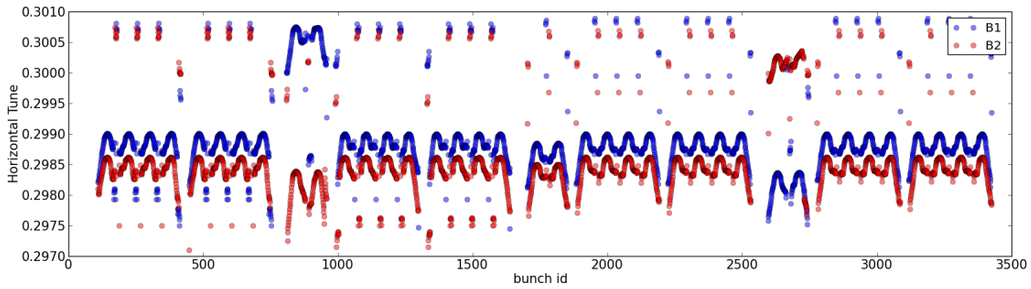

(a) Horizontal

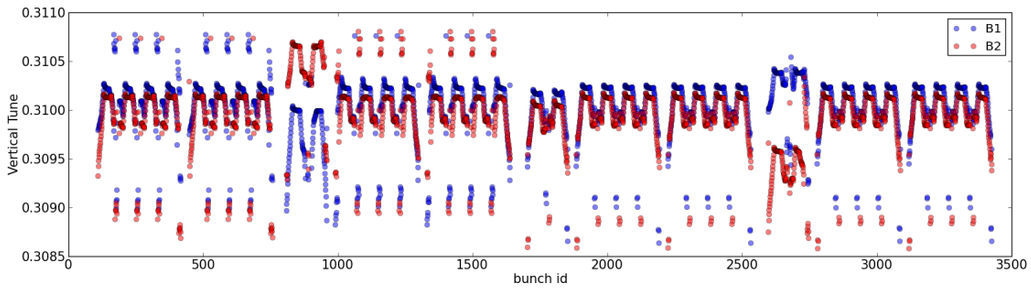

(b) Vertical

Figure 3: Bunch-by bunch tune at the start of collision for the nominal configuration with the standard filling scheme. The unperturbed fractional tunes are 0.31 and 0.32 in the horizontal and vertical planes respectively.

passively compensated in each plane [10]. Nevertheless the compensation is not perfect, it is therefore expected that a fraction of the estimated tune shift remains. Also, the contribution of long-range interactions in IPs 2 and 8 are not compensated. The precise values obtained with TRAIN in Tabs. 1 and 2 are consistent with these estimations. The bunch tune spread is significantly larger when considering all IPs mainly due to the missing offset interaction in IPs 2 and 8, as well as their long-range contributions. This effect can be observed in Fig. 3 by comparing the behaviour of the bunches in slots 800 to 990 and 2590 to 2770 which misses collision in either IP 2 or 8 due to the abort gap of the other beam, to the behaviour of the other bunches colliding in all IPs. One observes also in Fig. 3 a category of bunches with a significantly large tune shift difference at the edge of most of the trains. Those bunches are so-called super-Pacman, which are missing the offset collision at IPs 2 or 8. With an exact 4-fold symmetry of the filling scheme along with an 8-fold symmetry of the machine layout, all bunches would collide in all IPs. While these conditions are almost met in the LHC, the imperfections in the symmetry lead to missing head-on collision. As already visible in the orbit effect, the presence of an abort gap breaks this symmetry and generates two sets of consecutive super-Pacman bunches that could be identified. Here we also observed that the shift of IP8 by two slots with respect to the 8-fold symmetry point results in few super-Pacman bunches of IP8 at the edge of the bunch trains. Also, the optimisation of the filling scheme in order to maximise the luminosity in all experiments including the several constraints from the injector chain does not result in a perfectly 4-fold symmetric filling scheme, thus resulting in the super-Pacman of IP2, that consequently contributes to the bunch tune spread.
The bunch tune spreads predicted here for the different scenarios do not represent an issue as such. The tune variations are a concern for dynamic aperture and lifetime considerations, however due to the reduced number of long-range interactions the tolerance for Pacman and super-Pacman bunches are higher than for bunches experiencing all beam-beam interactions. As a result, Pacman and super-Pacman bunches were usually found to behave better than nominal bunches despite of their tune shift in the LHC [11, 12].

2.3 Chromaticity

While the dispersion is zero at the IP, a dispersion due to the crossing angle is unavoidable at the location of the long-range interactions. The resulting contribution to chromaticity is given by [9]:

$$\Delta Q'_{Xing} = -\Delta Q'_{//} = N_{LR}\frac{Nr_p}{\pi\varepsilon d_{Xing}^6}\eta d_{Xing}(d_{Xing}^2 - 3d_{//}^2) \tag{2.8}$$

with η the average dispersion at the location of the long-range interactions normalised to the beam size. The subscripts $_{Xing}$ and $_{//}$ identify quantities in the crossing plane and the plane normal to the crossing plane respectively. With a dispersion of 0.5 m, one finds that this contribution is negligible in all

configurations. The impact of the optics distortion due to the beam-beam interaction on the chromaticity correction with sextupoles is however significant. Indeed, considering only the quadrupolar component of the beam-beam interactions we can write the maximum β beating based on the corresponding tune shift introduced [3]:

$$\max \frac{\Delta\beta}{\beta} = \frac{2\pi\Delta Q}{\sin(2\pi Q)}. \tag{2.9}$$

Since the correction is proportional to the β function at the location of the sextupoles [3], we may obtain an upper bound for the resulting variation of the chromaticity corresponding to the least favourable phase advance between all beam-beam interactions and the sextupoles:

$$\left|\Delta Q'\right| < \left|(Q' - Q'_{nat})\frac{\Delta\beta}{\beta}\right|. \tag{2.10}$$

With a natural chromaticity $Q'_{nat} \approx -150$, we find that a chromaticity spread up to 1.6 units for the nominal scenario and up to 3 units for the ultimate due to long-range beam-beam interactions in IPs 1 and 5. On the other hand, a single head-on interaction may generate a chromaticity change up to 23 units. TRAIN simulations confirm that in the event of head-on collision in IPs 2 or 8, several units of chromaticity spread is expected for super-Pacman bunches of those IPs. Also, one observes in Fig. 4 that all bunches were shifted on average by several units of chromaticity, which is due to the effect of the head-on interactions in IPs 1 and 5. As will be discussed in Sec. 3, the tune shift due to the head-on interaction is largely dependent on the oscillation amplitude. As a result, there will be an important chromaticity spread within the bunch. This is not expected to be a concern for beam stability, however it does impact the long term stability of single particle trajectories and may affect for example beam lifetime.

On top of the head-on effect, a variation of the chromaticity for bunches at the head and tail of the trains is observed in Fig. 4, signature of a dependence on the long-range effect. Its amplitude of 2 to 3 units, however, does not match the prediction of Eqs. 2.8 and 2.10. Moreover, this contribution is not present at the end of the squeeze when the beams are separated at the IPs, indicating the contribution of head-on interaction. This combined effect of the long-range and head-on interactions on the chromaticity can be understood based on the chromaticity shift generated by a slightly offset collision at the IP generated by the long-range interaction together with an uncorrected residual dispersion at the IP in the order of few millimetres [9]:

$$\Delta Q' \approx -\frac{2\Delta Q_{HO}}{7d^3}\eta^*, \tag{2.11}$$

with η^* the dispersion at the IP normalised by the beam size. If needed this contribution can be reduced by correcting the residual dispersion at the IP under a millimetre, however similarly to the effect of β-beating on the chromaticity correction, this effect is highly amplitude dependent [9] and might not need a dedicated correction. Also, since this effect depends on the offset at the IP, it is expected to vanish for most bunches once the orbit is re-optimised such as to obtain the best maximum luminosity. However the chromaticity spread remains for Pacman bunches.

The chromaticity variations before the establishment of collision could be a concern for beam stability, however the effects considered here have a negligible impact on the chromaticity before the establishment of collision, as shown in Tabs. 1 and 2. The different orbits of the different bunches at the Landau octupoles could result in significant chromaticity variations through feed-down effect that are currently under investigations.

2.4 Linear coupling

Linear coupling is of interest mainly from the end of the ramp to the establishment of head-on collision due to its detrimental impact on the Landau damping effect generated by the octupoles [13]. Linear coupling is generated by beam-beam interactions with a transverse offset in both transverse planes. Starting from the expression of the beam-beam kick for round beams $\Delta x'$ [14], we find:

$$\frac{\partial\Delta x'}{\partial y}(x = d\cos(\alpha), y = d\sin(\alpha)) = \frac{\partial\Delta y'}{\partial x}(x = d\cos(\alpha), y = d\sin(\alpha)) \tag{2.12}$$

$$= -2\frac{r_0 N}{\gamma}\frac{(\sin(\alpha)\cos(\alpha)^3 + \cos(\alpha)\sin(\alpha)^3)d^2 + 2(1 - e^{d^2/2})\sin(\alpha)\cos(\alpha)}{e^{d^2/2}d^2} \tag{2.13}$$

$$\approx 4\frac{r_0 N}{\gamma}\frac{\sin(\alpha)\cos(\alpha)}{d^2}, \tag{2.14}$$

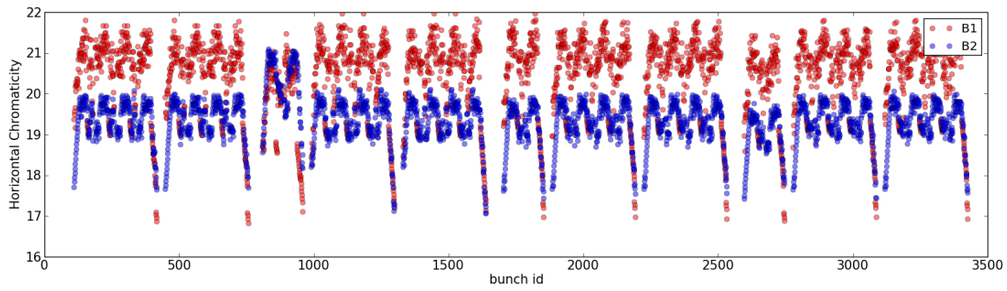

(a) Horizontal

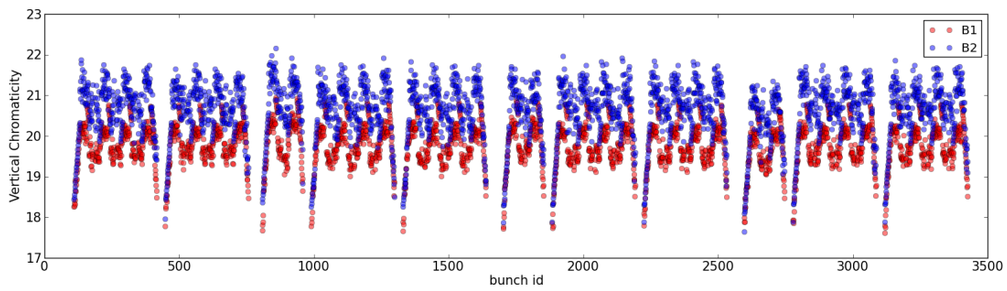

(b) Vertical

Figure 4: Bunch-by-bunch chromaticity at the start of collision for the nominal configuration with the standard filling scheme. The unperturbed chromaticity is 15 units in both planes.

Operational phase (β^*, scenario)	$\max \Delta X_{1,5}$ [σ]		$\max \Delta X_{tot}$ [σ]		$\max \Delta Q_{1,5}$ [10^{-3}]		$\max \Delta Q_{tot}$ [10^{-3}]		$\max \Delta Q'_{1,5}$		$\max \Delta Q'_{tot}$	
Filling scheme	H	V	H	V	H	V	H	V	H	V	H	V
Injection (6m, Nominal)												
Standard	0.25	0.3	0.42	0.37	0.2	0.2	2.2	2.0	0.0	0.0	0.1	0.1
BCMS	0.26	0.34	0.54	0.42	0.2	0.2	2.3	2.2	0.0	0.0	0.1	0.1
8b4e	0.23	0.22	0.35	0.29	0.2	0.2	1.9	1.7	0.0	0.0	0.1	0.1
End of the ramp and squeeze (64cm, Nominal)												
Standard	0.22	0.28	0.3	0.33	0.1	0.1	0.5	0.6	0.0	0.0	0.1	0.1
BCMS	0.19	0.32	0.29	0.37	0.1	0.1	0.6	0.6	0.0	0.0	0.0	0.0
8b4e	0.16	0.21	0.22	0.24	0.1	0.1	0.4	0.4	0.0	0.0	0.1	0.1
Start of collision (64cm, Nominal)												
Standard	0.22	0.29	0.31	0.34	0.7	0.8	3.4	2.1	4.2	3.0	5.1	3.3
BCMS	0.19	0.3	0.3	0.35	0.6	0.8	3.5	2.2	3.7	2.8	5.0	3.2
8b4e	0.14	0.2	0.24	0.24	0.4	0.4	3.2	2.2	3.4	2.2	4.2	2.8
End of the squeeze (41cm, Ultimate)												
Standard	0.19	0.26	0.26	0.3	0.1	0.1	0.5	0.5	0.0	0.0	0.1	0.0
BCMS	0.17	0.26	0.25	0.3	0.1	0.1	0.6	0.6	0.0	0.0	0.0	0.0
8b4e	0.14	0.17	0.19	0.2	0.1	0.1	0.4	0.4	0.0	0.0	0.1	0.1
Start of collision (41cm, Ultimate)												
Standard	0.27	0.36	0.36	0.41	1.1	1.1	3.9	2.1	3.0	3.2	3.9	4.3
BCMS	0.24	0.36	0.34	0.42	0.9	1.1	3.9	2.3	2.7	3.0	3.7	4.0
8b4e	0.18	0.25	0.27	0.28	0.6	0.6	3.5	2.1	2.2	2.5	2.9	4.2
Start of collision (15cm)												
Standard	0.21	0.28	0.29	0.32	0.6	0.7	3.3	2.0	1.8	2.2	2.6	2.5
BCMS	0.18	0.28	0.29	0.34	0.5	0.7	3.3	2.0	1.6	2.1	2.6	2.4
8b4e	0.14	0.19	0.22	0.23	0.3	0.4	3.1	2.0	1.2	1.6	1.9	2.3

Table 1: Estimations of the maximum bunch-by-bunch orbit, tune and chromaticity spread due to head-on, offset and long-range interactions for B1. The machine and beam parameters for the different scenarios can be found in [1]. An extra scenario beyond ultimate is also considered for which β^* levelling would not be used and the β^* at the start of collision is 15 cm, the other parameters are those of the ultimate scenario. The details of the standard and BCMS beams are also described in the note, the 8b4e scheme was considered here as well since its structure with many gaps reduces the overall spread significantly, the bunch intensity and emittance for this beam were assumed identical to the those of the BCMS beam.

Operational phase (β^*, scenario)	$\max \Delta X_{1,5}$ [σ]		$\max \Delta X_{tot}$ [σ]		$\max \Delta Q_{1,5}$ [10^{-3}]		$\max \Delta Q_{tot}$ [10^{-3}]		$\max \Delta Q'_{1,5}$		$\max \Delta Q'_{tot}$	
Filling scheme	H	V	H	V	H	V	H	V	H	V	H	V
Injection (6m, Nominal)												
Standard	0.26	0.31	0.39	0.66	0.1	0.2	2.1	2.3	0.0	0.0	0.0	0.1
BCMS	0.31	0.35	0.49	0.71	0.2	0.2	2.1	2.3	0.0	0.0	0.0	0.1
8b4e	0.21	0.24	0.32	0.49	0.2	0.2	1.7	1.9	0.0	0.0	0.0	0.1
End of the ramp and squeeze (64cm, Nominal)												
Standard	0.24	0.29	0.27	0.38	0.1	0.1	0.5	0.6	0.0	0.1	0.1	0.1
BCMS	0.24	0.32	0.29	0.41	0.1	0.1	0.6	0.6	0.1	0.1	0.1	0.1
8b4e	0.16	0.22	0.21	0.29	0.1	0.1	0.4	0.5	0.1	0.1	0.1	0.1
Start of collision (64cm, Nominal)												
Standard	0.23	0.29	0.28	0.43	0.8	0.7	3.7	2.2	3.2	3.7	4.0	4.5
BCMS	0.23	0.3	0.29	0.43	0.6	0.7	3.9	2.3	3.0	3.4	4.3	4.3
8b4e	0.15	0.21	0.22	0.32	0.4	0.4	3.7	2.4	2.2	3.0	3.6	3.9
End of the squeeze (41cm, Ultimate)												
Standard	0.21	0.26	0.24	0.35	0.1	0.1	0.5	0.6	0.1	0.1	0.1	0.1
BCMS	0.21	0.27	0.25	0.34	0.1	0.1	0.6	0.6	0.1	0.1	0.1	0.1
8b4e	0.14	0.18	0.18	0.24	0.1	0.1	0.4	0.5	0.1	0.1	0.1	0.1
Start of collision (41cm, Ultimate)												
Standard	0.28	0.36	0.32	0.48	1.2	1.1	4.2	2.2	3.8	3.3	4.7	3.9
BCMS	0.29	0.37	0.35	0.48	1.0	1.1	4.3	2.3	3.6	3.1	5.7	4.4
8b4e	0.19	0.26	0.25	0.36	0.6	0.6	4.0	2.4	2.9	2.6	4.9	3.7
Start of collision (15cm)												
Standard	0.22	0.28	0.26	0.41	0.7	0.7	3.5	2.1	2.5	2.2	3.5	2.9
BCMS	0.22	0.29	0.28	0.41	0.6	0.7	3.7	2.1	2.4	2.1	3.7	2.8
8b4e	0.15	0.2	0.21	0.31	0.4	0.3	3.5	2.3	1.8	1.6	2.9	2.3

Table 2: Estimations of the maximum bunch-by-bunch orbit, tune and chromaticity spread due to head-on, offset and long-range interactions for B2.

with α the roll angle of the interaction w.r.t. the horizontal plane. The last approximation holds for long-range interactions. This leads to a linear coupling strength [15]:

$$k = 2\frac{r_0 N}{\pi\varepsilon}\sum_{i}^{N_{LR}}\frac{\sin(\alpha_i)\cos(\alpha_i)}{d_i^2}. \tag{2.15}$$

Before establishing collision, i.e. at the end of the ramp or of the squeeze for the nominal and ultimate scenarios respectively, the combination of the parallel separation and crossing angle bumps generate long-range interactions on a skew plane, generating potentially a closest-tune-approach of $|C^-| \approx 2.5\cdot 10^{-4}$ per IR side, and therefore could generate a bunch coupling spread of the same order of magnitude. Since this is significantly smaller than the tune separation this effect does not represent an issue for beam stability if the orbit is well controlled. Nevertheless, recent measurements showed a long-range generated linear coupling up to $2\cdot 10^{-3}$ in the LHC, which is $\approx$10 times larger than expectations in the configuration of the experiment [16]. Orbit errors such as a roll angle error on the crossing angle plane could result in such an effect and could become unacceptable in the HL-LHC era. It is therefore crucial to understand the source of this discrepancy and gain control over it, since the bunch-to-bunch variation cannot be corrected using skew quadrupoles. Consequently, such a Pacman coupling effect could reduce the Landau damping of a subset of bunches and eventually lead to coherent instabilities.

3 Dynamic β effect

Based on Eq. 2.9, we find that a β-beating up to 14 % can be expected due to head-on beam-beam interactions at IPs 1 and 5 in the nominal scenario. MAD-X computations including head-on and long-range beam-beam interactions in all IPs are shown in Fig. 5. The amplitude of this effect was measured in the LHC by colliding high brightness bunches at injection energy [19] using AC-dipole measurement on colliding beams [20]. A correction scheme was proposed anticipating a potential need for correction [21], however its effectiveness could not yet be demonstrated experimentally.
Indeed, the contribution of the beam-beam interactions is close to the tolerance of 20% imposed by aperture and losses considerations [5] and does not leave sufficient margins for the remaining β-beating after correction of the bare optics [22]. Those tolerances are driven by the behaviour of particles at large amplitudes. For head-on beam-beam interactions the tune shift vanishes at large amplitude, the linear

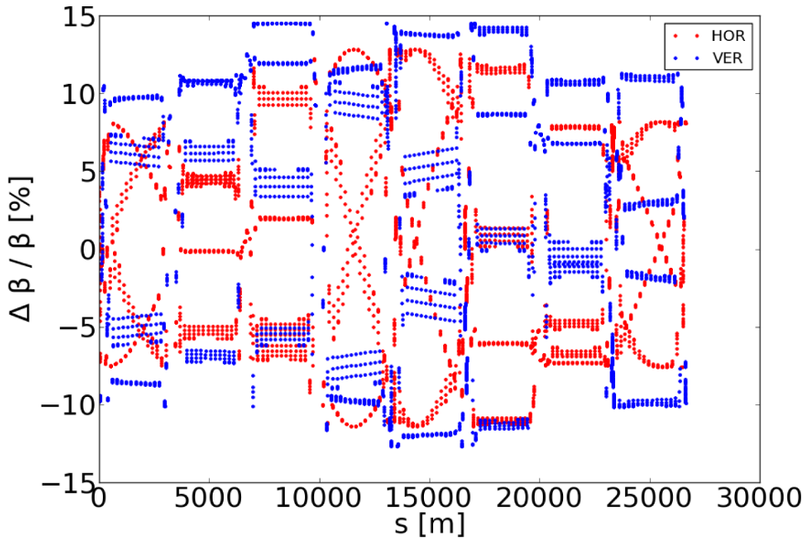

Figure 5: β-beating induced by beam-beam interactions in IPs 1 and 5 on beam 1 in the HL-LHC for zero amplitude particles [17], based on the last collision optics ($\beta^* = 15$ cm), with the nominal parameters at the start of collision, corresponding to a worst case senator. Nevertheless, since this effect is mainly driven by the head-on interaction, it is not expected to reduce when colliding at a larger β^*.

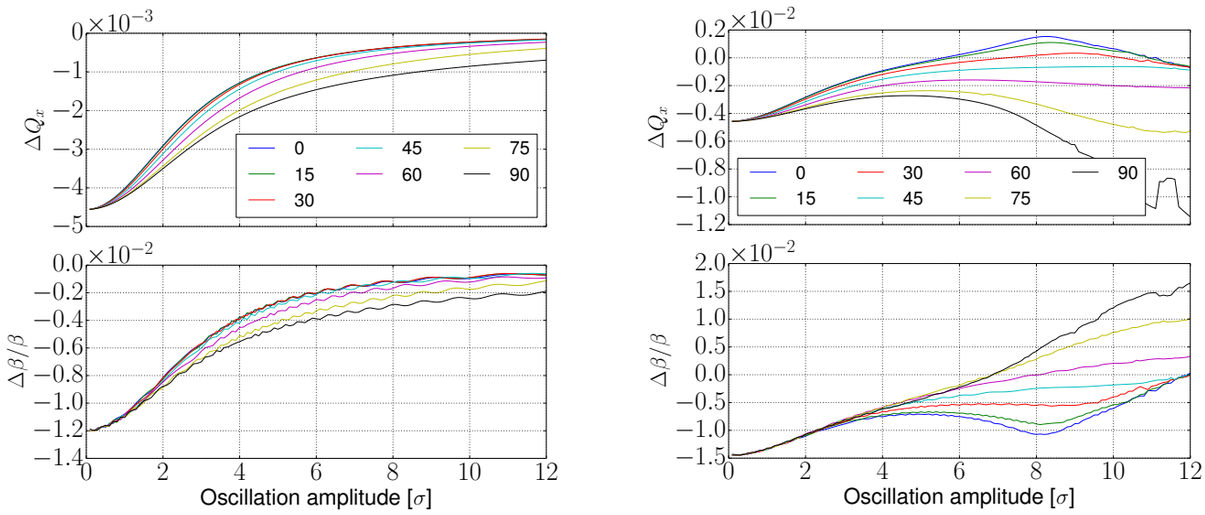

(a) Head-on

(b) Head-on and long-range

Figure 6: Tune shift and effective β-beating estimated with SVD of tracking data of particles oscillating at different amplitudes. The nominal LHC lattice was used, including the effect of head-on and long-range beam-beam interactions in IPs 1 and 5. While the amplitude of these effects are different for the HL-LHC configuration, the behaviour is similar [18].

theory is therefore not appropriate to describe this effect. A new method based on the singular value decomposition of single particle tracking data was developed in order to extend the optics functions to effective ones describing the non-linear, yet integrable, behaviour of the trajectory of particles oscillating at large amplitude [23]. Figure 6a shows the result of such an analysis for the LHC, using the parameters of the 2016 run. The effect of head-on interaction can be linearly scaled with the variation of the beam-beam tune shift in the HL-LHC with respect to the LHC. The effective β-beating vanishes along with the tune shift for particles oscillating at large amplitudes, due to the fact that the head-on beam-beam force vanishes away from the beam centre. In other words, despite the large tune shift for small amplitude particles, the effect on the tail is marginal, therefore a correction is not necessary to maintain the collimation performance in the tail. On the other hand the force due to long-range beam-beam interactions do not vanish away from the beam centre, therefore its impact on the particles oscillating at large amplitude may remain significant. Moreover, while the tune shift due to long-range beam-beam interactions is passively compensated by the alternating crossing angles in IPs 1 and 5 [10], the remaining β-beating depends on the phase advance between the IPs and can not be entirely mitigated. This effect is shown for the LHC in Fig. 6b. As opposed to the head-on interaction, the long-range interactions are not stronger in the HL-LHC w.r.t. the LHC since the crossing angle is adjusted to maintain the same dynamic aperture, consequently this effect is not expected to exceed a few percent of effective β-beating in the 6 σ transverse tails with nominal parameters. In pushed scenarios, e.g. with flat beams and/or compensating wires, such effects would need to be re-evaluated.

The distortion of the optics due to the beam-beam interaction at the IP may lead to a difference in the luminosity delivered to the two main experiments. Such an imbalance is unwanted and can, in both the nominal and ultimate scenarios, be mitigated by adjusting the levelling procedure individually in the two IPs, either with the β^* or with a transverse offset at the IP.

4 Coherent beam-beam modes

4.1 Stability

While inherently stable, the coherent beam-beam modes of oscillation may become unstable under the influence of the beam coupling impedance. In particular, it was demonstrated that strong mode coupling instabilities may arise when the frequency of the in-phase and out-of-phase dipole oscillations of the two beams (so-called σ and π-modes) reach the frequency of higher order head-tail modes [24]. This condition is already met in the present LHC, as the beam-beam parameter is larger than the synchrotron tune and will be met in the HL-LHC as well. Nevertheless a transverse feedback acting on the individual dipole mode of each bunch is sufficient to stabilise such instabilities in the LHC [24]. The efficiency of such a transverse feedback on the coupling of higher order mode head-tail is however not demonstrated and needed to be quantified. In particular, the HL-LHC relies on a low β^* in the two main IPs, resulting in significant synchrobetatron coupling due to the hourglass effect, allowing higher order head-tail modes to couple via the beam-beam forces [25, 26]. Alternative scenarios without crab cavities additionally feature a large crossing angle, with an even larger impact on synchrobetatron coupling. Excluding Landau damping, the stability of such modes can be estimated by numerical evaluation of the eigenvalue of the transverse one turn matrix, including coherent beam-beam forces, of the dynamical variable of a discretised longitudinal distribution, implemented for example in the code *BimBim* based on the circulant matrix model [27]. Figure 7 shows such estimations in the nominal configuration of the HL-LHC, along with self-consistent macro-particle simulations featuring a new parallelised implementation of the 6D coherent beam-beam kick extending Hirata's weak-strong model [28]. The implementation as well as discussions on the parametric dependence of this instability are detailed in [29]. While the agreement between the two models is clear for small beam-beam tune shift, the tracking simulations show a stabilisation of the coupled instability of the beam-beam π-mode and the azimuthal head-tail mode -1 when its frequency reaches the centre of the first lower side band of the incoherent spectrum. Such a stabilisation mechanism through Landau damping between synchrotron side bands was predicted theoretically without being quantified in the presence of beam coupling impedance [25]. For beam-beam parameters beyond the stabilisation by the lower side band, the Landau damping is sufficient to stabilise the beams. While encouraging, detailed analysis of the different configurations is still ongoing in order to ensure that such instabilities are stabilised in the presence of chromaticity, of a transverse feedback and of the crossing angle remaining due to the lack of crabbing strength after the re-baselining of the project in 2016 [1].

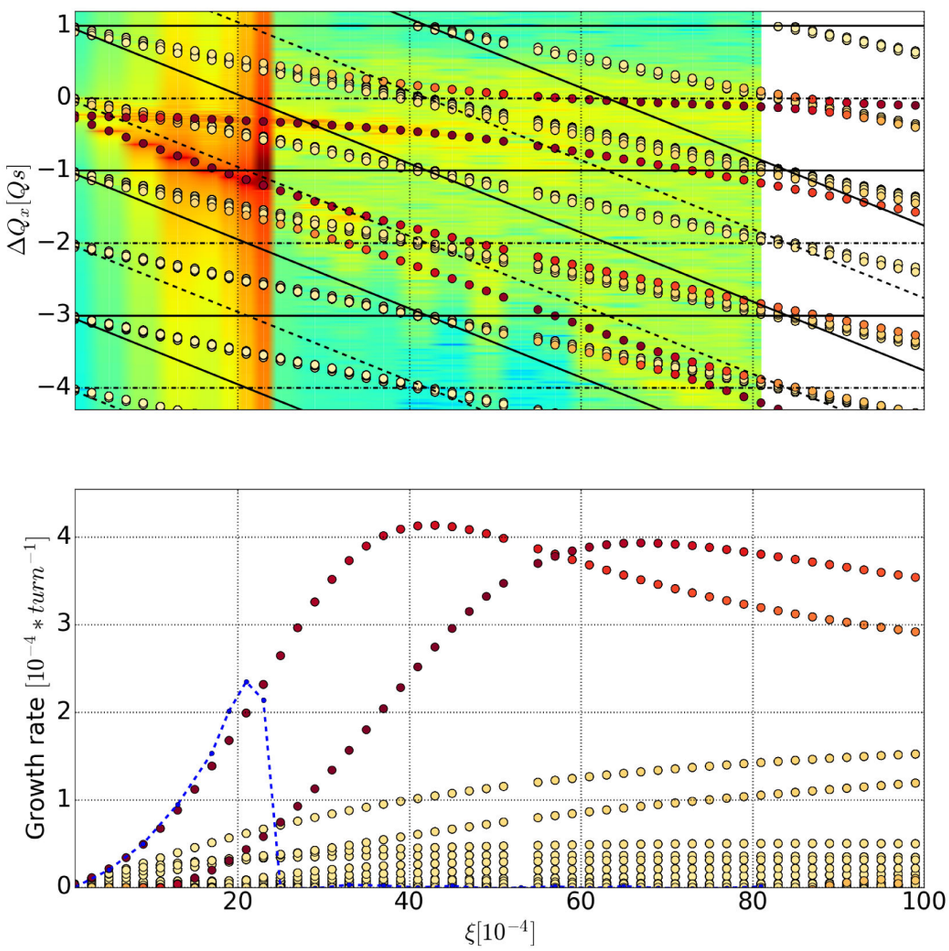

Figure 7: Real and imaginary tune shift of the coherent beam-beam modes of oscillation computed with circulant matrices (dots) and self-consistent macroparticle tracking simulations (spectrogram for the real part and blue line for the imaginary part). The upper boundary of the incoherent tune spectrum generated by the beam-beam interaction is represented by a horizontal black dashed line starting at 0 on the real part. The lower boundary is represented by a black dashed line starting from 0 and descending as the beam-beam tune shift increases. The synchrotron side bands of the incoherent spectrum are represented by repeating this pattern with a shift of $\pm nQ_s$, alternating dashed and solid lines. The configuration corresponds to obsolete HL-LHC nominal parameters with $\beta^* = 0.2$ and a single IP.

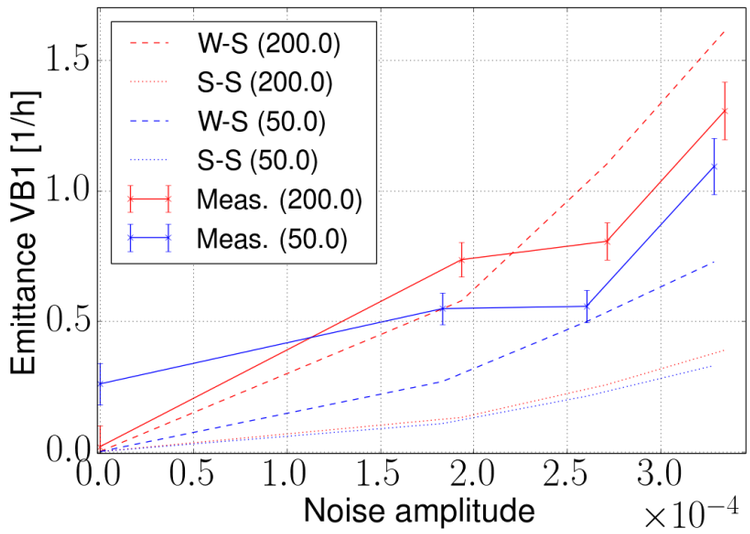

Figure 8: Measurement of the emittance growth due to a controlled external source of noise for beams colliding in IPs 1 and 5 in the LHC in 2016 (non-ATS optics, β^*=40 cm), with a beam-beam tune shift slightly above 0.02, and two different damper gains corresponding to a damping time of 50 (blue) and 200 (red) turns, for the vertical plane of B1. The details of the experiment can be found in [30]. The data are in coarse agreement with the weak-strong (W-S) model, but far from the strong-strong (S-S) model predictions, as expected since the phase advance are such that the coherent beam-beam modes are within the incoherent spectrum.

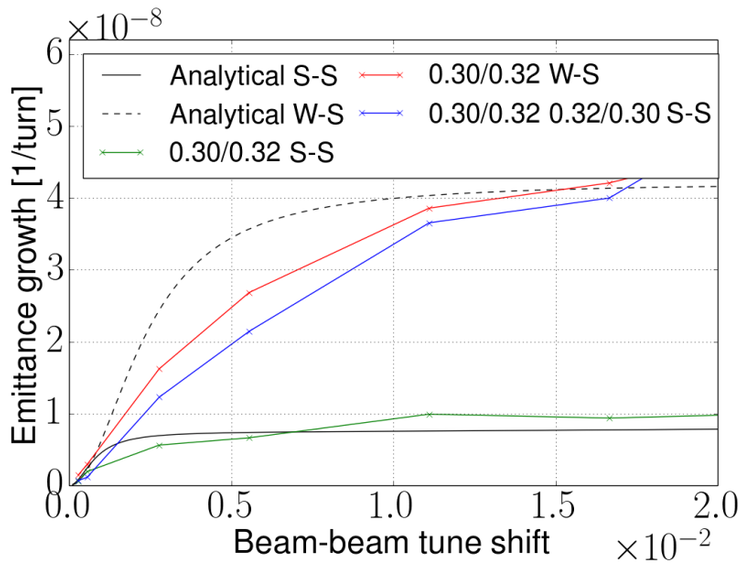

Figure 9: Comparison of the emittance growth simulated with COMBI [27] in the strong-strong (S-S) regime for two similar configurations, where the coherent beam-beam modes are moved out and in of the incoherent spectrum by implementing symmetric tunes in the two beams (green line) and by mirroring the tune of the two planes in the two beams (blue line). The expected mitigation of the emittance growth in the S-S regime (solid black line) [25] is obtained in simulations only in the symmetric configuration, whereas the emittance growth follows the analytical model based on the weak-strong (W-S) model (dashed black line) [31], as well as the COMBI simulations in the weak-strong regime (red line), in the configuration where the tunes are exchanged for the other beam, despite the strong-strong nature of the beam-beam interaction. The LHC is expected to behave according to the weak-strong prediction concerning the emittance growth even though the tunes are not mirrored for the two beams: Several other symmetry breaking parameters (phase advance between IPs, chromaticity, multiple IPs) lead to a similar behaviour.

	Beam 1		Beam 2	
	Horizontal	Vertical	Horizontal	Vertical
δ_0 [10^{-5}]	3.8	5.3	4.4	5.6
δ_{BPM} [10^{-5}]	220	250	190	210

Table 3: Fitted r.m.s. noise floor of the bare machine δ_0 and the ADT pickups δ_{BPM} normalised to the beam size.

4.2 Noise

An external source of noise, e.g. due to power converter ripple or ground vibrations, on a beam with a tune spread results in emittance growth. In the HL-LHC, the crab cavities are a potential source of noise in the transverse plane. The tolerances for the design of those cavities are based on a given maximum emittance growth and therefore on a beam dynamics model [31, 32]. Dedicated studies at the LHC demonstrated that the weak-strong model is appropriate to describe the behaviour of the emittance in nominal configurations of the LHC (Fig. 8), which can be interpreted as the result of the strong sensitivity of the strong-strong model to the machine and beam configuration. Figure 9 illustrates the change of regime from strong-strong to weak-strong when the coherent modes of oscillations are outside and inside of the incoherent spectrum. This effect was predicted analytically in [25] and detailed for LHC configurations in [33].

We can assume that the beams behave according to the following formula [31]:

$$\frac{1}{\varepsilon}\frac{d\varepsilon}{dt} = \frac{1}{2}\left(\delta_0^2 + G^2\delta_{BPM}^2\right)\left\langle \frac{4\pi^2\left(1-\frac{G}{2}\right)^2\Delta Q^2}{4\pi^2\left(1-\frac{G}{2}\right)\Delta Q^2 + \left(\frac{G}{2}\right)^2}\right\rangle, \tag{4.1}$$

where ε is the transverse emittance, δ_0 the r.m.s. noise floor of the machine normalised to the beam size, δ_{BPM} the r.m.s. noise floor of the transverse feedback pickup normalised to the beam size and G the transverse feedback gain, with $2/G$ the corresponding damping time. ΔQ is the tune shift of a single particle dependent on its actions, the average is then performed on all particles. In the following, we will evaluate this formula assuming that the tune shifts are normally distributed with an r.m.s. value corresponding to 0.168ξ, with ξ the beam-beam parameter [34]. Figure 10 shows the emittance growth rate measurement for different damper gains, showing a behaviour compatible with Eq. 4.1, the corresponding fitting parameters are reported in Tab. 3. Assuming that the noise arising from the damper is driven by the measurement noise of the signal of two pickups combined, the corresponding noise floor of the latter would be around 0.9 μm, which is compatible with their specifications [35]. The machine noise floor may be induced by ripple of the dipoles power converter, ripple of the quadrupole power converter with an offset of the beam orbit leading to feed down or vibrations of the quadrupoles. A detailed analysis of the different contributions combined with beam based estimations are needed to properly extrapolate the effect of the different sources to the HL-LHC, due to the various modifications with respect to the present LHC, in particular the increased β function in the arcs and in the triplet, as well as the introduction of crab cavities. Yet, assuming optimistically that the noise floor remains identical to the LHC, the contribution of the feedback noise becomes prohibitive with large beam-beam tune shifts, as shown by Fig. 11. Based on these considerations, it is clear that an upgrade of the damper pickup, reducing their noise floor by at least a factor 4, is needed to bring the emittance growth below the tolerated value of 1% integrated luminosity loss [1]. Since those estimates do not take into account the additional effect of the crab cavity noise, the performance of the ADT pickups have to be further improved to reach this goal [36]. Currently, it is planned to upgrade the acquisition electronics of the ADT pickup in order to achieve a reduction of the noise floor by a factor 10 [35].

5 Landau damping of single beam transverse instabilities

While the stability of coherent beam-beam modes of oscillation was covered in Sec. 4.1, we focus here on the effect of the beam-beam induced tune spread on the Landau damping of single beam instabilities driven by the impedance. In other words, the coherent aspects of the beam-beam force are neglected, to evaluate the incoherent effects on the beam stability. Such an assumption is valid in the presence of beam-beam interaction without synchrobetatron coupling, such as long-range beam-beam interactions or head-on interaction without crossing angle and in the presence of a strong feedback acting on the dipolar motion, thus suppressing the coherent interactions of the two beams.

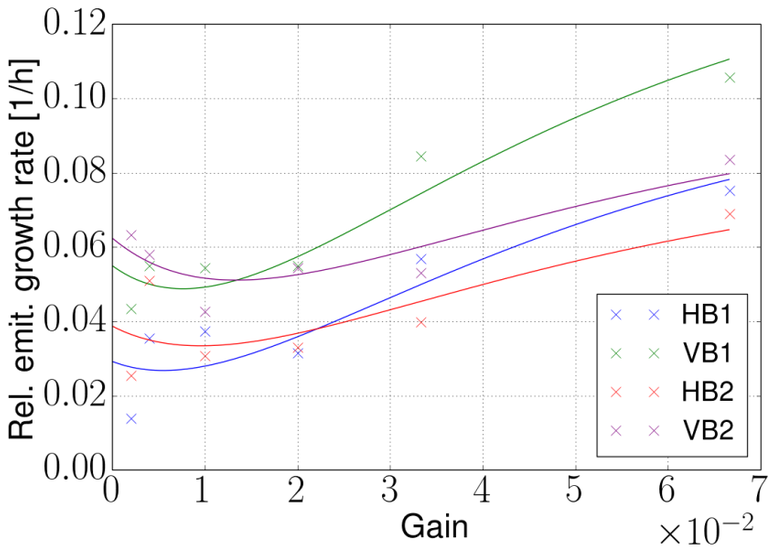

Figure 10: Measured relative emittance growth rate of the different bunches experiencing different gains (crosses) [37]. The contribution from IBS is subtracted based on the emittance growth of the non-colliding bunch. Since the non-colliding bunch of B2 experienced blow-up during the ramp, the growth rate of the non-colliding bunch of B1 is used instead. The curves show a fit using the weak-strong model (Eq. 4.1). The fit parameters are reported in Tab. 3.

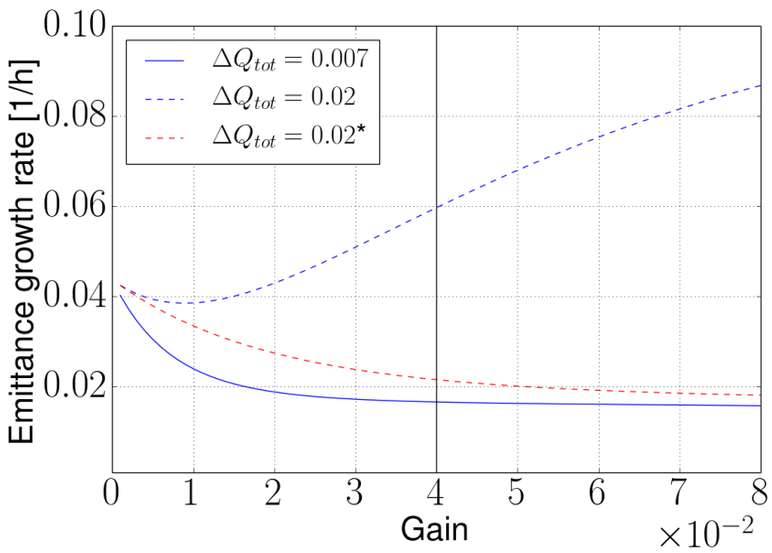

Figure 11: Extrapolation of the emittance growth due to the measured noise floor averaged over the beams and planes (Tab. 3) for the HL-LHC (dashed blue line), which correspond to the configuration of the test performed with a beam-beam parameter of 0.02. The large tune spread introduces a fast decoherence time and consequently reduces the feedback efficiency at mitigating the effect of the noise. In particular, at large gain, the noise introduced by the amplification of the pickup noise overcomes the beneficial effect of the ADT. With a reduced tune shift corresponding to the LHC in run II (solid blue line), the decoherence time is slow enough to allow the damper to mitigate the emittance growth to values compatible with observations [38, 39]. A vertical black line mark the operational damper gain in the LHC. The red dashed line show the HL-LHC extrapolation assuming an upgrade of the damper pickups leading to a reduction of their noise floor by a factor 4.

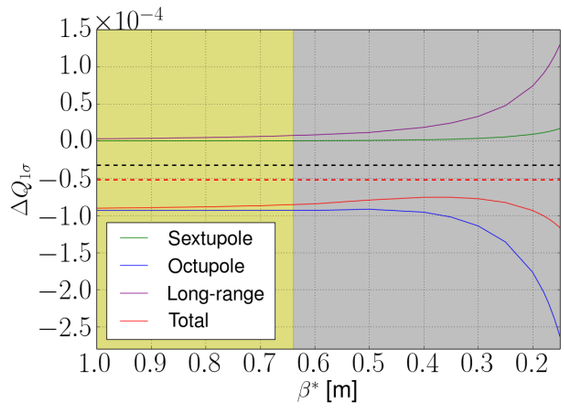

(a) Nominal (Standard filling scheme)

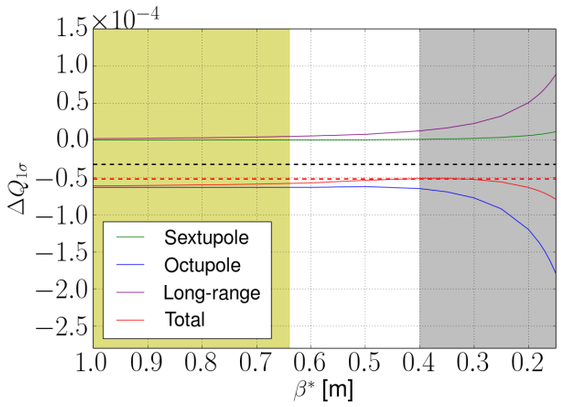

(b) Ultimate (BCMS)

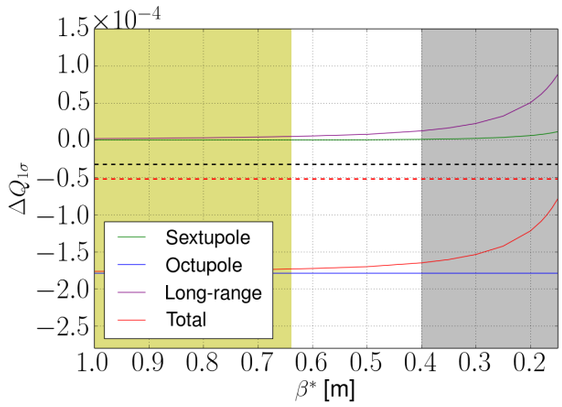

(c) Ultimate (BCMS) with Ramp and ATS (RATS) based on telescopic index of 3.3

Figure 12: R.m.s. tune spread generated by the octupoles at their maximum strength and by long-range beam-beam interactions as a function of β^* for different configurations of the HL-LHC, as defined in [1]. These estimates are based on the smallest transverse emittance, i.e. 2.1 μm for the nominal scenario with standard filling scheme and 1.7 μm for the ultimate scenario with BCMS beams. The areas shaded in yellow correspond to the part performed during the ramp. The tune spread is kept constant during the ramp at its minimum value at the end of the ramp by adjusting the octupole current. The areas shaded in grey corresponds to the squeeze performed in collision. During this phase, the model including octupole and the long-range interactions is no longer valid for bunches colliding head-on or with a small offset in one of the IPs. This approach remain valid considering pessimistically bunches that do not collide head-on in either of the IPs, yet experience the effect of the long-range interactions. The horizontal black and red dashed lines highlight the threshold derived for the single beam stability for the nominal and the non-upgraded collimators respectively [1].

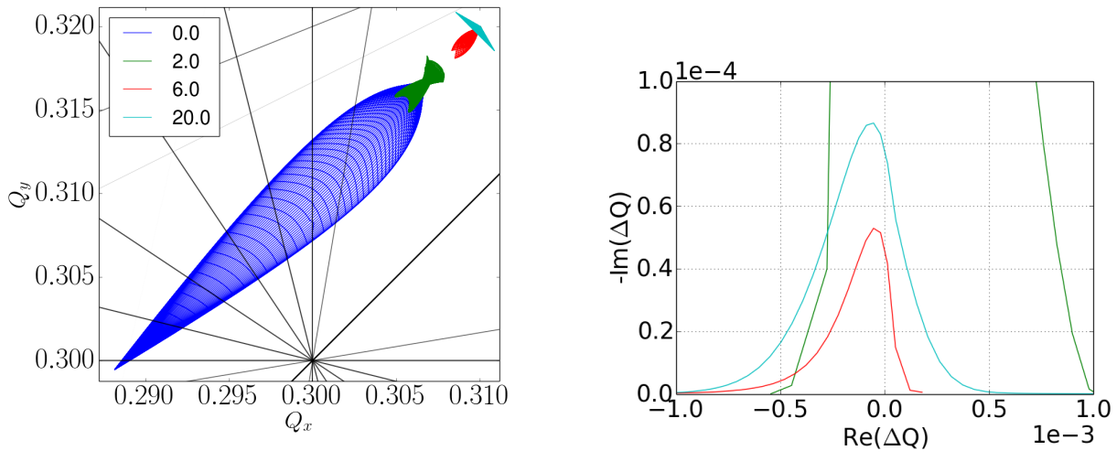

(a) Tune footprint

(b) Stability diagram

Figure 13: Tune footprints and stability diagrams with different normalised separation between the beams at the IP in the nominal configuration of the HL-LHC at the start of luminosity production. The stability diagram corresponding to head-on collision (blue curve) is significantly out of scale.

5.1 Long-range

The amplitude detuning generated by both octupoles and long-range beam-beam interactions can be reasonably well approximated by their linear contribution with the action [2, 40]. The resulting r.m.s. tune spread is then proportional to the strength of Landau damping for the head-tail modes driven by the impedance. Figure 12 shows the evolution of these contributions, including the effect of the sextupoles, to the tune spread during the cycle, evaluated by tracking with MAD-X, using the HL-LHC thin lens optics V1.3 and with the octupoles powered at their maximum strength. This quantity therefore represents the maximum of the Landau damping that can be obtained with the available hardware during the process, which has to be compared with the estimations of single beam requirement. The most critical point of the cycle from the point of view of coherent stability occurs before the collisions are established, since the contribution of the head-on beam-beam interactions then dominates over the contributions of the octupoles and of the long-range interactions. The part of the cycle shaded in grey in Fig. 12 does not consider this important contribution to Landau damping which will be discussed in the next section.
In the nominal scenario (Fig. 12a), β^* levelling starts right at the end of the ramp, where the long-range contribution is still weak. For this configuration, the two beams considerations on the octupole current do not differ significantly from the single beam ones. We consider now the most critical scenario in terms of beam stability, the ultimate scenario with a reduced emittance thanks to the BCMS beam. In such a configuration, the upgrade of the collimators with low resistivity coatings is critical to maintain the beam stability through the squeeze down to $\beta^* = 41$ cm (Fig. 12b). Nevertheless, experience at the LHC suggests that the operation is robust with a factor 2 margin in the octupole current [41]. The ultimate scenario with the collimator upgrade lies just below this margin. The operational margins are mainly driven by the uncertainty on the impedance model itself as well as the tight control of the linear coupling and of the lattice non-linearities needed to ensure the required tune spread. As detailed in the next section, the margins are further reduced when collapsing the separation bumps. The latter can be recovered by introducing the telescopic part of the ATS optics [42] during the energy ramp, as the normalised physical aperture in the arc increases, thus allowing for a boost of tune spread for the same octupole current already at the end of the ramp (Fig. 12c).

5.2 Head-on with an offset

When bringing the beams into collision, the beam-beam force at the IP varies significantly from a long-range type of interaction to a head-on type of interaction, with a strong impact on the amplitude detuning illustrated on Fig. 13a. The r.m.s. tune spread is not sufficient to provide an accurate estimate of the Landau damping effect in these conditions, as illustrated by the corresponding stability diagrams computed numerically from the tracking simulation [43] shown in Fig. 13b. In order to accurately represent the margin in terms of beam stability in these configuration where the shape of the stability diagram varies significantly, we use the coherent stability factor which corresponds to the multiplicative factor that would bring the tune shift of all the coherent modes of oscillation obtained with the linearised model to the stability area. This factor was estimated during the process of bringing the beams into collision based on the tune footprint estimated with MAD-X and the corresponding stability diagram computed

with PySSD, along with the coherent modes of oscillation obtained with DELPHI with the impedance model of the HL-LHC at flat top including the crab cavity impedance and the low impedance collimators [1]. The results are summarised in Fig. 14. The estimations on the right-hand side of the plots correspond to the configuration studied in previous section up to the establishment of collision (Gray area in Fig. 12). The reduction of the separation between the beams constitutes the transition to the regime dominated by the tune spread of head-on beam-beam interaction characterised by large stability margins, visible on the left side of the plot in all configurations. In all cases, this transition goes to a minimum of stability when reaching a total separation of $\approx 1.5\ \sigma$, which is driven by the change of sign of the tune spread within the core of the beam producing the largest contribution to Landau damping [43]. In the nominal configuration, the stability factor for this minimum of stability remains below 0.5, i.e. sufficient margins w.r.t. the instability threshold only if the crab cavities are switched on before the collapse of the separation bumps. Another minimum of stability is visible at a total separation of $\approx 6\ \sigma$, which is due to the increase of the strength of the long-range beam-beam interactions as the separation bump is collapsed leading to a reduction of the tune footprint visible in Fig. 13a and consequently of the stability diagram as the separation between the beams decreases. This effect is counter balanced by the effect of the beam-beam interaction with a small offset at the IP, which starts to dominate the tune spread below this separation. In the nominal configuration, this minimum of stability still leaves enough operational margins.
The ultimate configuration is more critical, since as discussed in previous section, the margins are already critical at the end of the squeeze. The increase of the strength of the long-range beam-beam interaction due to the collapse of the separation bumps already leads to an unstable configuration around 8 to 10 σ total separation (Fig. 14c). The second minimum at smaller separation also requires the crab crossing to be enabled before the collapse of the separation bumps, nevertheless the operational margins are again reduced.

Figures 14b and 14d show the same two configurations, where the current in the octupoles was artificially increased beyond their capacity in order to obtain sufficient margins with respect to the instability threshold through the whole cycle. This increase of the tune spread, and therefore of Landau damping, can be obtained by increasing of the β function at the octupoles thanks to the ATS optics, to overcome the limitation of theirstrength. Such an effect can reasonably be achieved thanks to a small telescopic index of ≈ 1.7 [44] in the nominal and ultimate scenario. Larger telescopic indices are needed in absence of the low impedance collimator upgrade.
The minimum of stability at large separation is fully suppressed by this measure since the effect of the long-range interaction is largely overcompensated by the octupoles. While such an overcompensation might have an detrimental effect on the dynamic aperture, an intermediate telescopic index adjusted to compensate the effect of the long-range interactions on the tune spread would be sufficient and meet dynamic aperture requirements. Thus, for the ultimate scenario an equivalent current of -750 A, corresponding to a telescopic factor of ≈ 1.6 would be sufficient to maintain the operational margin. The minimum of stability at smaller separation is not as strongly affected by this mitigation since it is mainly driven by the presence of the head-on beam-beam interaction, which affects the amplitude detuning in a very different way w.r.t. the octupoles. Nevertheless, the increased tune spread in the tails thanks to the stronger octupoles is beneficial and brings the minimum to an acceptable level. In order to maintain strictly the operational margin, an equivalent octupole strength of -1000 A would be sufficient, corresponding to a telescopic index of ≈ 2.2. Since this implies a significant increase of the tune spread, a verification of the impact on dynamic aperture is required.

In case the measures proposed to maximise the beam stability could not be put in place and a critical point has to be crossed during the process, the speed of execution of the collapse of the separation bumps has to be maximised in order to prevent the development of an instability. The speed of the collapse of the separation was estimated at 1.6 to 2.0 σ/s in the nominal and ultimate scenario respectively [45]. A few seconds are therefore spent at the first minimum of stability in the range ≈ 10 to $6\ \sigma$, which is comparable to the fastest instability rise time expected With such a speed, it is expected that the minimum of stability at small separation is crossed in less than a second, much faster than the expect instability rise times of a few seconds [45]. While the second minimum is narrower in beam separation, ≈ 2 to $1.5\ \sigma$, the speed of the separation bump reduces towards the end of its execution to allow for a smooth operation of the superconducting magnets, the speed is reduced to $\approx 0.3\ \sigma$/s [45]. Thus also about a second is spent in the critical configuration, assuming that the reproducibility of the separation bump is sufficient such as to ensure a collision below $1.5\ \sigma$ at the end of the process. If this condition is not met, minutes can be spent in this configuration until the luminosity optimisation process, allowing for an instability to develop. The study presented here considers the most critical configuration where the separation bumps are collapsed in the two IPs simultaneously. In case of issues, past studies suggest that collapsing the separation bumps asynchronously in the two IPs, or introducing separation bumps in the same plane for

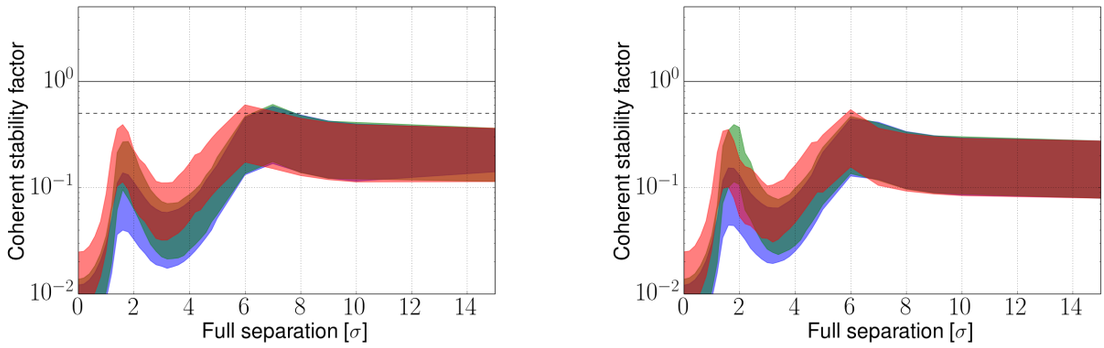

(a) Nominal, $I_{oct} = -570$ A

(b) Nominal, $I_{oct} = -750$ A

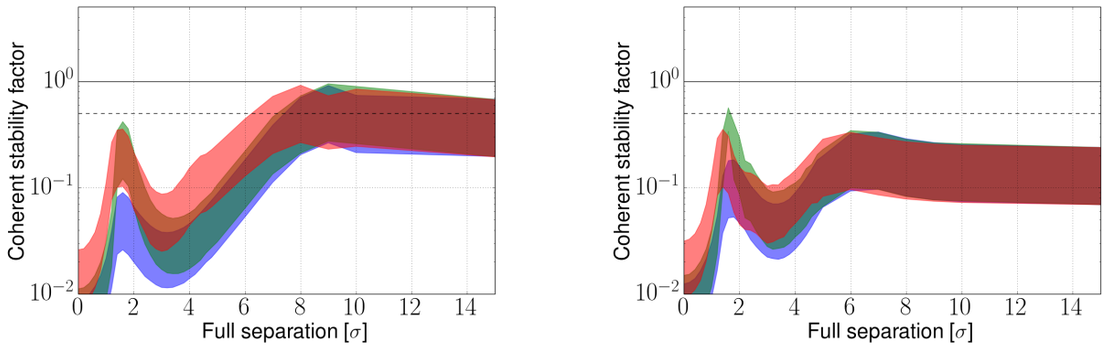

(c) Ultimate, $I_{oct} = -570$ A

(d) Ultimate, $I_{oct} = -1000$ A

Figure 14: Coherent stability factors varying the separation between the beams at IPs 1 and 5 simultaneously for different configurations of the HL-LHC. The impedance model includes the crab cavity impedance and the upgraded collimators. The area represent the error bar due to variations of the chromaticity (both due to the reproducibility of the machine and to bunch to bunch variations). The blue areas correspond to simulation with a full crab crossing enabled since the beginning of the process, the green area to a maximum crab angle of 180μrad (nominal) and the red to the absence of crabbing. Consistently with the estimations in [1], Gaussian transverse distributions corresponding to an emittance of 2.5 μm and cut at 3 σ are considered.

the two IPs may lead to a beneficial effect on the beam stability thanks to the different behaviour of the amplitude detuning in the two planes [43]. Based on those arguments, it seems that improvements of the implementation of the separation bumps, in terms of speed or shape, could allow for a mitigation of the minimums of stability. However those solutions are not considered as robust as an increase of the effective octupole strength.

6 Conclusion

The bunch-by-bunch variations of orbit, tune and chromaticity are mostly within tolerances for both the nominal and ultimate scenarios. The orbit effect in the triplet was identified as a potential issue as it exceeds the tolerance for static offsets. Nevertheless, the bunch-by-bunch variations of the orbit may have a reduced impact with respect to static offsets depending on the failure scenarios considered, therefore this effect has to be further detailed in order to define a tolerance on this type of effect specifically. In case the tolerance had to be increased to account for this effect, this would have an impact on the β^* reach. The linear coupling variations were also identified as potential issue to maintain the beam stability. Since this effect depends strongly on the alignment of the crossing angles bumps in the different IPs, its control will rely on measurement and correction of the orbit in the interaction region with tolerances to be defined.
While large for particles oscillating at small amplitude, the optics distortion due to the head-on beam-beam interaction vanishes at large amplitude and is therefore not a concern for beam cleaning and does not impact significantly the estimations performed in the various failure scenarios. The effect of the long-range beam-beam interactions on the particles at large amplitude is expected to be tolerable.
The beam stability is mostly critical at the end of the ramp or at the end of the squeeze for the nominal and ultimate scenarios respectively, as well as during the process of bringing the beams into collision. In the ultimate scenario the beam stability is marginal due to the compensation of the tune spread of the Landau octupoles by long-range beam-beam interactions and to the offset collision at the IP when brining the beams into collision. While acceptable on paper with the low-impedance collimator upgrade, this scenario does not leave any operational margin. These margins are currently needed for operation of the LHC. Their understanding and possible reduction are the topic of numerous theoretical and experimental

Separation [σ]	Equivalent octupole current [A] (Telescopic index)					
	Nominal			Ultimate		
	CFC	LS2 upg.	Full upg.	CFC	LS2 upg.	Full upg.
6-10	-1250 (2.6)	-1000 (2.2)	-750 (1.7)	-1020 (2.2)	-900 (2.0)	-780 (1.7)
1.5-2	-2500 (3.9)	-1000 (2.2)	-750 (1.7)	-2750 (4.2)	-900 (2.0)	-780 (1.7)

(a) $\varepsilon = 2.5\mu$m

Separation [σ]	Equivalent octupole current [A] (Telescopic index)					
	Nominal			Ultimate		
	CFC	LS2 upg.	Full upg.	CFC	LS2 upg.	Full upg.
6-10	-1500 (2.9)	-1200 (2.5)	-1000 (2.2)	-1500 (2.9)	-1250 (2.6)	-1100 (2.3)
1.5-2	-2300 (3.8)	-1300 (2.8)	-1000 (2.2)	-2600 (4.0)	-1250 (2.6)	-1100 (2.3)

(b) $\varepsilon = 1.7\mu$m

Table 4: Minimum octupole current requirement to maintain the beam stability through the collapse of the separation bump with operational margins, for the nominal and ultimate scenarios with CFC and upgraded low impedance collimators. The LS2 upgrade corresponds to a replacement of 4 secondary collimators (TCSGs) of IR7 with new designs based on a Molybdenum coated Molybdenum-Graphite bulk (TCSPMs) and 2 primary collimators (TCPs) of IR7 with an uncoated Molybdenum-Graphite bulk (TCPPMs). The full upgrade includes the replacement of the remaining 5 CFC secondary collimators in IR7. Consistently with the estimations in [1], Gaussian transverse distributions corresponding to an emittance of 2.5 μm (upper table) and cut at 3 σ are considered. In the lower plot, it is assumed that the smallest transverse emittance of 1.7μm can be maintained until collision. A margin of a factor two with respect to the estimated stability threshold is taken into account.

investigations. Nevertheless, it is worth noting that the margins can be recovered by anticipating the telescopic squeeze during the ramp, such as to increase the effect of the octupoles during the critical phases. The requirements for the different scenarios are summarised in Tab. 4.
The transverse dampers both mitigate the emittance growth caused by various noise sources present in the machine and introduce additional noise by feeding the pickup measurement noise into the beam. Its operation at high gain is therefore optimal only with a low measurement noise. While acceptable in the LHC due to the reduced beam-beam tune shift w.r.t. the HL-LHC, a dedicated experiment with high brightness single bunches shows that the noise from the damper will lead to a significant emittance growth, unless an upgrade of the pickups is performed in order to reduce their noise floor by at least a factor 4.

7 Acknowledgements

The authors would like to thank G. Arduini, R. De Maria, R. Tomàs and S. Redaelli for fruitful discussions, A. Gorzawksi and M. Hostettler for their important contributions to the TRAIN code, as well as D. Valuch and the operation teams of the LHC and its injectors for the great support for experimental studies. The contributions from D. Amorim, S. Antipov, N. Bianccaci and B. Salvant on the impedance, wake fields and single beam stability thresholds were also essential for this study.
This research was supported by the HL-LHC project. The authors are also grateful for the high performance computing resources made available by CERN's IT department as well as by EPFL's Laboratoire de Physique des Accélerateur de Particules.

References

[1] E. Métral, S. Antipov, F. Antoniou, R. Appleby, G. Arduini, J. Barranco, P. Baudrenghien, N. Biancacci, C. Bracco, R. Bruce, X. Buffat, R. Calaga, L. Carver, M. Crouch, R. D. Maria, S. Fartoukh, D. Gamba, M. Giovannozzi, P. Gonçalves Jorge, W. Hofle, G. Iadarola, N. Karastathis, A. Lasheen, K. Li, T. Mastoridis, L. Medina, A. Mereghett, D. Mirarchi, B. Muratori, S. Papadopoulou, Y. Papaphilippou, D. Pellegrini, T. Pieloni, S. Redaelli, G. Rumolo, B. Salvant, E. Shaposhnikova, M. Solfaroli, C. Tambasco, R. Tomàs, and D. Valuch, *Update of the HL-LHC Operational Scenarios for Proton Operation*, CERN-ATS-Note-2018 (CERN, Geneva, Switzerland, 2018).

[2] D. Neuffer and S. Peggs, *Beam-beam tune shift and spreads in the SSC - Head on, long range and PACMAN conditions*, SSC-63 (Superconducting Super Collider Laboratory, Dallas, USA, 1986).

[3] A. W. Chao and M. Tigner, *Handbook of Accelerator Physics and Engineering* (World Scientific, Singapore, 1999).

[4] W. Herr, *Tune shifts and spreads due to short and long range beam-beam interactions in the LHC*, CERN-LHC-Note-119 (CERN, Geneva, Switzerland, 1990).

[5] R. Bruce, C. Bracco, R. De Maria, M. Giovannozzi, S. Redaelli, R. Tomas Garcia, F. M. Velotti, and J. Wenninger, *Updated parameters for HL-LHC aperture calculations for proton beams*, CERN-ACC-2017-0051 (CERN, Geneva, 2017).

[6] E. Yamakawa, P. Baudrenghien, R. Calaga, R. Apsimon, and A. C. Dexter, "Crab cavity studies including full detuning and offsets due to long range beam-beam interactions," Presented at the 7th HL-LHC Collaboration Meeting, Madrid, Spain `https://indico.cern.ch/event/647714/contributions/2768967/attachments/1557095/2449950/wp4-crab-cavity.pdf` (14th Nov, 2017).

[7] https://espace.cern.ch/HiLumi/WP2/Shared%20Documents/Filling%20Schemes%20HL-LHC/25ns_2760b_2748_2494_2572_288bpi_13inj.csv (2018).

[8] https://espace.cern.ch/HiLumi/WP2/Shared%20Documents/Filling%20Schemes%20HL-LHC/25ns_2748b_2736_2258_2374_288bpi_12inj.csv (2018).

[9] B. Erdélyi and T. Sen, *Analytic Studies of the Long Range Beam-Beam Tune Shifts and Chromaticities*, FERMILAB-TM-2171 (FERMILAB, Batavia, IL 60510, 2002).

[10] W. Herr, *Features and implications of different LHC crossing schemes*, LHC-Project-Report-628 (CERN, Geneva, 2003).

[11] W. Herr, X. Buffat, R. Calaga, R. Giachino, G. Papotti, T. Pieloni, and D. Kaltchev, "Long-range beam-beam effects in the LHC," in *Proceedings of the ICFA Mini-workshop on beam-beam effects in hadron colliders*, Geneva, Switzerland, 18-22 March 2013, edited by W. Herr and G. Papotti (CERN, Geneva, Switzerland, 2014) pp. 211–216.

[12] X. Buffat, G. Arduini, E. Bravin, G. Iadarola, E. Métral, Y. Papaphilippou, D. Pellegrini, S. Redaelli, B. Salvachua, M. Solfarloli, G. Trad, D. Valuch, J. Wenninger, J. Barranco, T. Pieloni, and C. Tambasco, "Long-range and head-on beam-beam interactions : What are the limits ?" in *Proceedings of the 2016 Evian workshop on LHC beam operation*, Evian-les-Bains, France, 13-15 Dec. 2016, edited by B. Goddard, S. Dubourg, and G. Trad (CERN, Geneva, Switzerland).

[13] L. Carver, D. Amorim, N. Biancacci, X. Buffat, K. Li, E. MÃl'tral, B. Salvant, and M. Schenk, "Destabilising effect of linear coupling in the lhc," in *Proceedings of IPAC2017*, Copenhagen, Denmark, 14-19 May. 2017, edited by G. Arduini, M. Lindroos, J. Pranke, V. Schaa, and M. Seidel (Jacow, Geneva, Switzerland).

[14] W. Herr, "Beam-beam interactions," in *CAS - CERN Accelerator School: Intermediate Course on Accelerator Physics*, Zeuthen, Germany, 15-26 September 2003, edited by D. Brandt (CERN, Geneva, Switzerland, 2006) pp. 379–410.

[15] F. Ruggiero, G. Rumolo, F. Zimmermann, and Y. Papaphilippou, *Beam Dynamics Studies for Uniform (Hollow) Bunches or Super-bunches in the LHC: Beam-beam effects, Electron Cloud, Longitudinal Dynamics, and Intrabeam Scattering*, LHC-Project-Report-627 (CERN, Geneva, 2003).

[16] J. Wenninger, X. Buffat, F. S. Carlier, J. M. Coello De Portugal Martinez Vazquez, K. Fuchsberger, M. Hostettler, T. H. B. Persson, R. Tomas Garcia, D. Valuch, and A. Garcia-Tabares Valdivieso, *LHC MD2877: Beam-beam long range impact on coupling measurements*, CERN-ACC-NOTE-2018-0026 (CERN, Geneva, Switzerland, 2018).

[17] T. Pieloni, X. Buffat, L. Medina, C. Tambasco, R. Tomas, J. Barranco, and P. Gonçalves Jorge, "Dynamic β and β-beating effects in the presence of the beam-beam interactions," in *Proceedings of HB2016*, Malmö, Sweden, 3-8 Jul. 2016 (Jacow, Geneva, Switzerland).

[18] L. Medina, X. Buffat, R. Tomas, J. Barranco, and T. Pieloni, "Correction of linea and non-linear optics errors due to beam-beam with multipoles for the HL-LHC," in *Proceedings of IPAC2018*, Vancouver, Canada, 29 Apr. -4 May 2018 (Jacow, Geneva, Switzerland).

[19] P. Gonçalves Jorge, J. Barranvo, T. Pieloni, X. Buffat, F. Carlier, J. Coello de Portugal, E. Fol, L. Medina, R. Thomas, and A. Wegscheider, "Measurement of β-beating due to strong head-on beam-beam interactions in the LHC," in *Proceedings of IPAC2017*, Copenhagen, Denmark, 14-19 May. 2017, edited by G. Arduini, M. Lindroos, J. Pranke, V. Schaa, and M. Seidel (Jacow, Geneva, Switzerland).

[20] R. Tomás, X. Buffat, S. White, J. Barranco, P. Gonçalves Jorge, and T. Pieloni, "Beam-beam amplitude detuning with forced oscillations," Phys. Rev. Accel. Beams **20**, 101002 (2017).

[21] L. Medina, R. Tomas, X. Buffat, Y. Papaphilippou, J. Barranco, and T. Pieloni, "Correction of β-beating due to beam-beam for the lhc and its impact on dynamic aperture," in *Proceedings of IPAC2017*, Copenhagen, Denmark, 14-19 May. 2017, edited by G. Arduini, M. Lindroos, J. Pranke, V. Schaa, and M. Seidel (Jacow, Geneva, Switzerland).

[22] F. S. Carlier, J. M. Coello De Portugal Martinez Vazquez, S. Fartoukh, E. Fol, D. Gamba, A. Garcia-Tabares Valdivieso, M. Giovannozzi, M. Hofer, A. S. Langner, E. H. Maclean, L. Malina, L. E. Medina Medrano, T. H. B. Persson, P. K. Skowronski, R. Tomas Garcia, F. Van Der Veken, and A. Wegscheider, *Optics Measurements and Correction Challenges for the HL-LHC* , CERN-ACC-2017-0088 (CERN, Geneva, 2017).

[23] P. Gonçalves Jorge and X. Buffat, *Computation of Optics Distortions due to Beam-Beam Interactions in the FCC-hh*, CERN-THESIS-2016-317 (CERN, Geneva, Switzerland, 2016).

[24] S. White, X. Buffat, N. Mounet, and T. Pieloni, "Transverse mode coupling instability of colliding beams," Phys. Rev. ST Accel. Beams **17**, 041002 (2014).

[25] Y. Alexahin, "A study of the coherent beam-beam effect in the framework of Vlasov perturbation theory," Nucl. Instrum. Methods Phys. Res. A **480**, 253 (2002).

[26] X. Buffat, J. Barranco, T. Pieloni, and C. Tambasco, "Effect of the crossing angle on coherent stability," Presented at the HL-LHC WP2 meeting `https://indico.cern.ch/event/563293/contributions/2316566/attachments/1352296/2041874/2016-09-20-expanded.pdf` (11th Nov. 2016).

[27] X. Buffat, *Transverse beams stability studies at the Large Hadron Collider*, Ph.D. thesis, EPFL (2015).

[28] K. Hirata, H. Moshammer, and F. Ruggiero, "A symplectic beam-beam interaction with energy change," Part.Accel. **40**, 205 (1993).

[29] L. Barraud and X. Buffat, "Mode coupling instability of colliding beams in the HL-LHC," To be published (2018).

[30] X. Buffat, N. Biancacci, S. Furuseth, D. Jacquet, E. Métral, D. Pellegrini, M. Pojer, G. Trad, D. Valuch, J. B. T. Pieloni, C. Tambasco, and J. Qiang, *Probing the behaviour of high brightness bunches in collision at 6.5 TeV and the interplay with an external source of noise (MD1433)*, CERN-ACC-NOTE-2017-0030 (CERN, Geneva, Switzerland, 2017).

[31] V. A. Lebedev, "Emittance growth due to noise and its suppression with the feedback system in large hadron colliders," AIP Conference Proceedings **326**, 396 (1995).

[32] P. Baudrenghien and T. Mastoridis, "Transverse emittance growth due to RF noise in the high-luminosity LHC crab cavities," Phys. Rev. ST Accel. Beams **18**, 101001 (2015).

[33] T. Pieloni, *A Study of Beam-Beam Effects in Hadron Colliders with a Large Number of Bunches*, Ph.D. thesis, EPFL (2008).

[34] G. Stupakov, V. Parkhomchuk, and V. Shiltsev, *Decoherence of a Gaussian Beam Due to Beam-Beam Interaction*, SSCL-Preprint-495 (Superconducting Super Collider Laboratory, Dallas, USA, 1993).

[35] D. Valuch, "On improving the ADT pickup resolution," Presented at the HL-LHC WP2 meeting `https://indico.cern.ch/event/718322/contributions/2952007/attachments/1629790/2597412/On_improving_the_ADT_pick_up_resolution.pdf` (10th Apr. 2018).

[36] P. Baudrenghien, R. Calaga, T. Mastoridis, and E. Yamakawa, "Crab cavities, RF noise and operational aspects (counter-phasing, full detuning). an update," Presented at the HL-LHC WP2 meeting https://indico.cern.ch/event/645814/contributions/2622537/attachments/1475139/2291024/Meeting_13_06_2017.pdf (13th Jun. 2017).

[37] X. Buffat, S. V. Furuseth, S. Kostoglou, B. M. Salvachua Ferrando, P. S. Papadopoulou, L. Ponce, M. Solfaroli Camillocci, R. Suykerbuyk, D. Valuch, D. J. Walsh, J. Barranco Garcia, and T. Pieloni, *Impact of the ADT on the beam quality with high brightness beams in collision (MD2155)*, CERN-ACC-NOTE-2018-0005 (CERN, Geneva, 2018).

[38] F. Antoniou, M. Hostettler, G. Iadarola, S. Papadopoulou, Y. Papaphilippou, D. Pellegrini, and G. Trad, "Can we predict luminosity?" in *Proceedings of the 2016 Evian workshop on LHC beam operation*, Evian-les-Bains, France, 13-15 Dec. 2016, edited by B. Goddard, S. Dubourg, and G. Trad (CERN, Geneva, Switzerland).

[39] S. Papadopoulou, F. Antoniou, G. Arduini, E. Bravin, I. Efthymiopoulos, M. Hostettler, G. Iadarola, N. Karastathis, Y. Papaphilippou, D. Pellegrini, and G. Trad, "Emittance, intensity and luminosity modeling and evolution," in *Proceedings of the 2017 Evian workshop on LHC beam operation*, Evian-les-Bains, France, 12-14 Dec. 2017, edited by T. Argyropoulos, S. Dubourg, and G. Trad (CERN, Geneva, Switzerland).

[40] J. Gareyte, J.-P. Koutchouk, and F. Ruggiero, *Landau damping, dynamic aperture and octupole in LHC*, LHC Project Report 91 (CERN, Geneva, Switzerland, 1997).

[41] X. Buffat, G. Arduini, D. Amorim, S. Antipov, L. Barraud, N. Biancacci, F. Giordano, G. Iadarola, G. Mazzacano, E. Métral, B. Salvant, M. Soderen, and D. Valuch, "Our understanding of the instabilities and mitigation tools/strategy," in *Proceedings of the 2017 Evian workshop on LHC beam operation*, Evian-les-Bains, France, 12-14 Dec. 2017, edited by T. Argyropoulos, S. Dubourg, and G. Trad (CERN, Geneva, Switzerland).

[42] S. Fartoukh, "Achromatic telescopic squeezing scheme and application to the lhc and its luminosity upgrade," Phys. Rev. ST Accel. Beams **16**, 111002 (2013).

[43] X. Buffat, W. Herr, N. Mounet, T. Pieloni, and S. White, "Stability diagrams of colliding beams in the large hadron collider," Phys. Rev. ST Accel. Beams **17**, 111002 (2014).

[44] S. Fartoukh *et al.*, "Achromatic telescopic squeezing (ATS) scheme: principle, by-products and experience with beams," Presented at the LHC Performance Workshop, Chamonix, France https://indico.cern.ch/event/676124/contributions/2775564/attachments/1590966/2517768/Cham2018_SF.pptx (30th Jan, 2018).

[45] C. Tambasco, J. Barranco, N. Biancacci, X. Buffat, T. Pieloni, and B. Salvachua, "Specification of separation collapsing speed for HL-LHC," Presented at the HL-LHC WP2 meeting https://indico.cern.ch/event/463032/contributions/1979649/attachments/1259995/1861804/HL_LHC_collapse_update.pdf (19th Apr. 2016).